Ni et al. *Zool. Res.* 2022, 43(6): 989−1004
https://doi.org/10.24272/j.issn.2095-8137.2022.278

ZR | Zoological Research

Article Open Access

Chronic lithium treatment ameliorates ketamine-induced mania-like behavior via the PI3K-AKT signaling pathway

Rong-Jun Ni[1], Tian-Hao Gao[1], Yi-Yan Wang[1], Yang Tian[1], Jin-Xue Wei[1], Lian-Sheng Zhao[1], Pei-Yan Ni[1], Xiao-Hong Ma[1], Tao Li[2,3,4,*]

[1] *Psychiatric Laboratory and Mental Health Center*, *West China Hospital of Sichuan University*, *Chengdu*, *Sichuan* 610041, *China*
[2] *Affiliated Mental Health Center & Hangzhou Seventh People's Hospital*, *Zhejiang University School of Medicine*, *Hangzhou*, *Zhejiang* 310013, *China*
[3] *NHC and CAMS Key Laboratory of Medical Neurobiology*, *MOE Frontier Science Center for Brain Science and Brain-machine Integration*, *School of Brain Science and Brain Medicine*, *Zhejiang University*, *Hangzhou*, *Zhejiang* 310014, *China*
[4] *Guangdong-Hong Kong-Macao Greater Bay Area Center for Brain Science and Brain-Inspired Intelligence*, *Guangzhou*, *Guangdong* 510799, *China*

ABSTRACT

Ketamine, a rapid-acting antidepressant drug, has been used to treat major depressive disorder and bipolar disorder (BD). Recent studies have shown that ketamine may increase the potential risk of treatment-induced mania in patients. Ketamine has also been applied to establish animal models of mania. At present, however, the underlying mechanism is still unclear. In the current study, we found that chronic lithium exposure attenuated ketamine-induced mania-like behavior and c-Fos expression in the medial prefrontal cortex (mPFC) of adult male mice. Transcriptome sequencing was performed to determine the effect of lithium administration on the transcriptome of the PFC in ketamine-treated mice, showing inactivation of the phosphoinositide 3-kinase (PI3K)-protein kinase B (AKT) signaling pathway. Pharmacological inhibition of AKT signaling by MK2206 (40 mg/kg), a selective AKT inhibitor, reversed ketamine-induced mania. Furthermore, selective knockdown of AKT via AAV-AKT-shRNA-EGFP in the mPFC also reversed ketamine-induced mania-like behavior. Importantly, pharmacological activation of AKT signaling by SC79 (40 mg/kg), an AKT activator, contributed to mania in low-dose ketamine-treated mice. Inhibition of PI3K signaling by LY294002 (25 mg/kg), a specific PI3K inhibitor, reversed the mania-like behavior in ketamine-treated mice. However, pharmacological inhibition of mammalian target of rapamycin (mTOR) signaling with rapamycin (10 mg/kg), a specific mTOR inhibitor, had no effect on ketamine-induced mania-like behavior. These results suggest that

Received: 15 September 2022; Accepted: 17 October 2022; Online: 18 October 2022

Foundation items: This study was supported by the Key Project of the National Natural Science Foundation of China (81920108018 to T.L. and P.S.), Ministry of Science and Technology of the People's Republic of China (2022ZD0205200), Natural Science Foundation of Sichuan Province (2022NSFSC1607), Key R & D Program of Zhejiang (2022C03096 to T.L.), Special Foundation for Brain Research from Science and Technology Program of Guangdong (2018B030334001), and Project for Hangzhou Medical Disciplines of Excellence & Key Project for Hangzhou Medical Disciplines

*Corresponding author, E-mail: litaozjusc@zju.edu.cn

chronic lithium treatment ameliorates ketamine-induced mania-like behavior via the PI3K-AKT signaling pathway, which may be a novel target for the development of BD treatment.

Keywords: Lithium; Ketamine; Medial prefrontal cortex; Bipolar disorder; Manic; PI3K-AKT signaling pathway

INTRODUCTION

According to the World Health Organization (WHO) World Mental Health (WMH) Survey, more than 1% of the world's population suffers from bipolar disorder (BD) (Alonso et al., 2011; Cardoso et al., 2018). BD is characterized by major mood swings, including emotional highs (mania) and lows (depression) (Grande et al., 2016). Mania is typified by hyperactivity, irritability, hypersexuality, decreased need for sleep, and cognitive deficits (Young et al., 2011).

Interestingly, a previous case report has described the development of hypomania- and mania-like symptoms in a patient receiving ketamine therapy for reflex sympathetic dystrophy (Ricke et al., 2011). Additionally, evidence from clinical case reports has shown that ketamine infusion increases the risk of treatment-emergent mania in non-psychiatric patients (Mandyam & Ahuja, 2017; Nichols et al., 2016). Clinical reports have also found that ketamine administration can alleviate depressive symptoms of major depressive disorder (MDD) and BD within minutes but may cause manic symptoms in non-psychiatric patients. These findings indicate that the affective switch is associated with ketamine use (McInnes et al., 2016).

Accumulating evidence suggests that acute and chronic ketamine-induced mania-like behaviors in rodents can mimic the clinical symptoms of BD (Debom et al., 2016; Ettenberg et al., 2020; Gao et al., 2021; Ghedim et al., 2012; Spohr et al., 2022). Recent studies have used lithium and valproate as effective therapeutics for ketamine-induced mania-like behaviors in rats (Ettenberg et al., 2020; Ghedim et al., 2012) and mice (Gao et al., 2021). However, the molecular mechanism underlying the effects of lithium treatment on ketamine-induced mania-like behavior remains unclear.

Several studies have shown that lithium inhibits inositol monophosphatase and decreases the synthesis of inositol triphosphate, thereby regulating protein kinase B (AKT) to promote cell growth, proliferation, and anabolism (Hermida et al., 2017; Malhi & Outhred, 2016; Zhang et al., 2022). Moreover, lithium has been shown to enhance AKT phosphorylation and inhibit glycogen synthase kinase-3 (GSK-3) (Beaulieu et al., 2004; Liu et al., 2013). Male transgenic mice overexpressing GSK-3beta display mania-like behaviors and up-regulated AKT expression in the brain (Prickaerts et al., 2006). In addition, mice with deletion of GSK-3beta in the brain mimic antipsychotic efficacy and behaviors (Urs et al., 2012), while lithium treatment increases behavioral responses in GSK-3beta heterozygous mice (Beaulieu et al., 2008; Urs et al., 2012). Previous studies have shown that the N-methyl-D-aspartate receptor (NMDAR) antagonist ketamine activates the α-amino-3-hydroxy-5-methyl-4-isoxazolepropionic acid receptor (AMPAR), which regulates phosphoinositide 3-kinase (PI3K) and AKT (Cavalleri et al., 2018). Ketamine can also rapidly activate the AKT-mammalian target of the rapamycin (mTOR) signaling pathway, leading to increased synaptic proteins and spine synapses in the medial prefrontal cortex (mPFC) of rats (Li et al., 2010). In BD, the mPFC is characterized by a decrease in volume, neuronal size, and glial cell density, as well as changes in gene expression (Savitz et al., 2014). However, the roles of the PI3K-AKT signaling pathway in ketamine-induced mania-like behavior remain largely unknown.

In this study, we utilized high-throughput transcriptome sequencing to investigate the molecular mechanisms regulating the effects of lithium on ketamine-induced mania in mice. Furthermore, we used pharmacological and genetic manipulations to explore the role of the PI3K-AKT signaling pathway in ketamine-induced behaviors.

MATERIALS AND METHODS

Animals

Adult male C57BL/6 mice (8 weeks old) were purchased from Chengdu Dossy Experimental Animals (Jianyang, China). The mice were housed in an animal facility with food and water available *ad libitum* and were maintained on a normal 12 h light/dark cycle (lights on at 0700h, lights off at 1900h). All procedures were performed in accordance with the Institutional Animal Care and Use Committee of Sichuan University (Approval No.: 2021270A). The guidelines used in the present study were followed to minimize animal suffering and the number of animals used.

Drugs

Ketamine (National Institutes for Food and Drug Control, China) and lithium chloride (Sigma Aldrich, USA) were separately dissolved in saline solution (vehicle). Rapamycin (HY-10219), LY294002 (HY-10108), MK2206 dihydrochloride (HY-10358), and SC79 (HY-18749) were obtained from MedChem Express (MCE, USA). Rapamycin, LY294002, and MK2206 dihydrochloride were dissolved in 10% dimethyl sulfoxide (DMSO) and saline solution (vehicle), while SC79 was dissolved in a saline solution containing 10% DMSO and 10% sulfobutylether-β-cyclodextrin (SBE-β-CD, vehicle). Lithium chloride (47.5 mg/kg (Chaves Filho et al., 2020), twice daily for 8 days), ketamine (20 mg/kg (Crawford et al., 2020), single dose), rapamycin (10 mg/kg (Xing et al., 2019), daily for 3 days), LY294002 (25 mg/kg (Xing et al., 2019), daily for 2 days), MK2206 dihydrochloride (40 mg/kg (He et al., 2020), daily for 3 days), and SC79 (40 mg/kg (Su et al., 2014), daily for 3 days) were intraperitoneally (i.p.) injected into mice according to weight.

The dosages of chronic lithium treatment were based on previous studies (Hopkins & Gelenberg, 2000; Ishii et al., 2021; Katz et al., 2022; Shvartsur et al., 2022) indicating safe and therapeutic lithium plasma levels (≥0.4 mEq/L). According to our previous study (Gao et al., 2021), plasma analysis showed a lithium plasma level of 0.0484±0.0022 mEq/L in the control group and 0.5523±0.1615 mEq/L in the lithium-treated group, maintained within the patient therapeutic range, i.e., 0.4

mEq/L to 1.0 mEq/L (Ishii et al., 2021). Therapeutic lithium levels in plasma can be maintained at ≥0.5 mEq/L for >2 h after a single administration lithium or chronic lithium treatment in rodents (Morrison et al., 1971).

Stereotaxic surgery

Adult mice were deeply anesthetized using 1% pentobarbital sodium (60 mg/kg, i.p.). The mouse head was fixed in a digital stereotaxic frame (Stoelting Company, USA). The incisor bar was adjusted until the heights of the lambda and bregma skull points were equal to achieve a flat skull position. A sagittal incision was made along the midline of the head. Mice were stereotaxically implanted with two guide cannulas (RWD, China) bilaterally in the mPFC with the following coordinates (anteroposterior: +1.80 mm from interaural line, mediolateral: ±0.30 mm from midline, dorsoventral: −2.10 mm from dura) (Franklin & Paxinos, 2007). The tips of the guide cannulas were positioned 0.5 mm dorsal to the injection site. Three stainless steel screws and the guide cannulas were fixed to the skull with dental cement. Two dummy cannulas were inserted into the two guide cannulas to prevent clogging and infection. After surgery, all mice were allowed to survive for 7 days and were then euthanized.

Adeno-associated virus-mediated gene transfer

AKT knockdown was performed using an adeno-associated virus (AAV) selectively expressing AKT-short hairpin RNA with enhanced green fluorescent protein (AAV-AKT-shRNA-EGFP). First, the coding regions of AKT were amplified from mouse cDNA by polymerase chain reaction (PCR) and cloned into pAAV-U6-shRNA-CMV bGlobin-eGFP-3Flag. These recombinant plasmids were then packaged into AAV9 particles together with an AAV helper plasmid (pAAV) and purified by CsCl density gradient centrifugation and ultrafiltration. These procedures were conducted by GeneChem (China). The titers of the recombinant AAV supernatant were determined by quantitative PCR: AAV-AKT-shRNA-EGFP (AKT-shRNA), 1.22×10^{13}; AAV-Control-shRNA-EGFP (Control-shRNA), and 1.17×10^{13} (genome copies/mL), diluted to 5×10^{12} before the experiments. The scrambled AKT-shRNA and Control-shRNA sequences are 5'-GGCCC AACACCTTTATCAT-3' and 5'-CCATGATTCCTTCATATT TGC-3', respectively.

At least one week after stereotaxic surgery, intra-mPFC infusions of AAV-Control-shRNA-EGFP/AAV-AKT-shRNA-EGFP into the cannulas were performed bilaterally at a rate of 0.2 μL/min (1 μL/side) using a 10 μL Hamilton syringe connected to a dual-channel syringe pump (RWD Life Science, China) via injection needle extending 0.5 mm below the guide cannula into the mPFC. At the end of each injection, the injection needle was left in place for an additional 10 min. All mice were allowed to survive for three weeks and were then euthanized.

Behavioral testing

Before behavioral testing, each mouse was handled for 2 min per day for 3 days for habituation to experimental manipulation. On the day of testing, all mice were allowed to acclimate to the behavioral testing room for 30 min before behavioral testing. The mice were tested successively using the open-field test (OFT) and elevated plus-maze (EPM) test. All tests were performed between 0900h and 1700h under dim light. The recorded videos were analyzed using EthoVision (v12.0) tracking software (Noldus, Netherlands). Except for OFT described in Figure 1, all behavioral tests were performed within 20 min of ketamine administration.

Open-field test

Five minutes after ketamine administration, the OFT was applied to evaluate locomotor exploration in mice, as described previously (Ni et al., 2020a). The open-field apparatus was a square arena (40 cm×40 cm×35 cm) consisting of a white Plexiglas box. Each mouse was placed in the corner and permitted to explore the apparatus for 5 min freely. After each test, the open-field apparatus was cleaned with a 75% alcohol solution to remove any trace of odor. During the 5 min test period, total distance moved, total cumulative duration of not moving (velocity<1.75 cm/s), time spent in the center zone, and number of center entries in the OFT were analyzed using the video tracking system (Noldus, Netherlands).

Elevated plus-maze test

Each mouse was subjected to the EPM test to evaluate anxiety-related behavior, with additional information on motor activity (Dawson & Tricklebank, 1995). The EPM was constructed of a white Plexiglas box with two opposite-set open arms (30 cm×7 cm, length×width) and two opposite-set closed arms (30 cm×7 cm×16 cm, length×width×height) in a plus configuration, elevated 60 cm above the ground. A video camera was fixed above the EPM to record movements for analysis. The mice were individually placed at the center of the EPM, facing one of the closed arms, and allowed to freely explore the apparatus for 5 min. The apparatus was cleaned with a 75% alcohol solution after each trial to remove any trace of odor. During the 5 min test period, the video tracking system was used to quantify the total distance moved, total cumulative duration of not moving (velocity<1.75 cm/s), number of arm entries, and time spent on the open arms.

Tissue preparation

To investigate the quantitative levels of c-Fos in the mPFC, the mice were transcardially perfused 120 min after ketamine injection. At 120 min post single injection, the c-Fos signal can peak in the brain, as confirmed in mice previously (Xiu et al., 2014). The mice were transcardially perfused with 0.9% sodium chloride and 4% paraformaldehyde (PFA) in phosphate-buffered saline (PBS; 0.1 mol/L; pH 7.4), with whole brains then removed, post-fixed in 4% PFA, dehydrated through sucrose solution, and sectioned at 40 μm on a Leica microtome (Leica CM3050S, Germany).

Antibody characterization and immunohistochemistry

The specificity of the primary antibody rabbit anti-c-Fos (D120415, Sangon Biotech, China) has been tested extensively (Gao et al., 2021; Li et al., 2019).

To identify the activated regions in the mPFC of each group, we used immunocytochemistry to examine the expression levels of c-Fos, a molecular marker of neuronal activity. The brain sections were processed as described previously (Gao

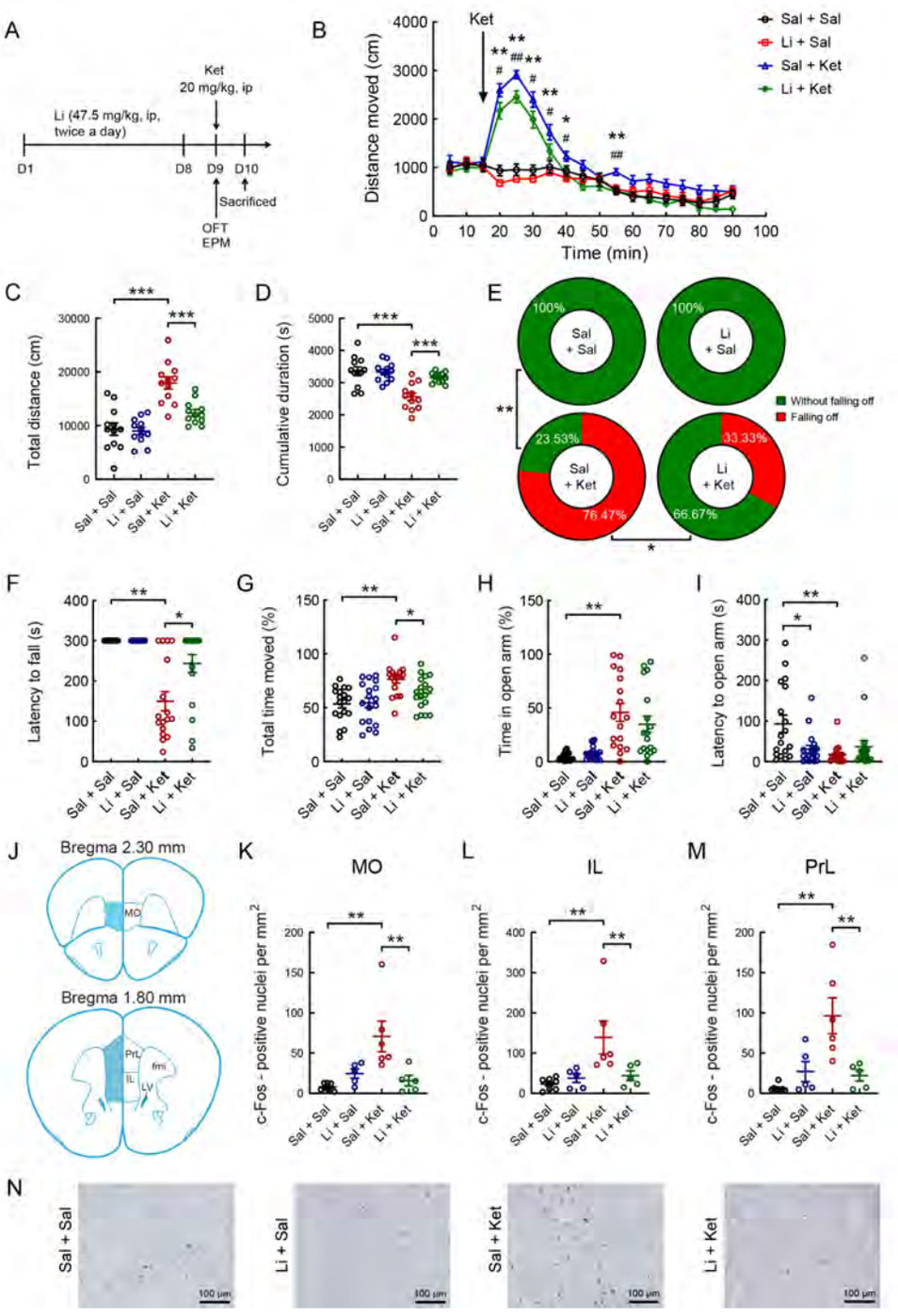

Figure 1 Effects of lithium on ketamine-induced mania-like behavior and density of c-Fos-positive neurons induced by ketamine in the mPFC of mice

A: Timeline of the experiment. B: Line plots depict distance traveled in the open field arena as a function of 5 min bins during 90 min open-field session before and after single administration of ketamine or saline in lithium- or saline-treated mice. Sal+Sal vs. Sal+Ket: *: P<0.05; **: P<0.01; Li+Ket vs. Sal+Ket: $^{\#}$: P<0.05; $^{\#\#}$: P<0.01 (n=12, each group). C: Total distance moved during 75 min open-field session. D: Total cumulative duration of immobility (velocity<1.75 cm/s) during 75 min open-field session. E: Percentage of mice that fell off the platform during 5 min EPM test (green, without falling off; red, falling off). F: Latency to fall off open arms in each group (n=17–18, each group). G: Percentage of cumulative duration of movement (moving, velocity>1.75 cm/s) in the EPM. H: Percentage of time spent in open arms during 5 min EPM test. I: Latency to open arms in each group. J: Anatomical organization of the mPFC, including the MO, IL, and PrL. K–M: Density of c-Fos-positive neurons in the MO, IL, and PrL of each group (Sal+Sal: n=8, Li+Sal: n=5, Sal+Ket: n=6, Li+Ket: n=5). N: High-magnification photomicrograph illustrating c-Fos immunoreactivity in the PrL of each group. Scale bars: 100 μm in E. Ket, ketamine; Li, lithium; Sal, saline. *: P<0.05; **: P<0.01; ***: P<0.001.

et al., 2021), with sequential incubation in permeating solution (0.3% hydrogen peroxide and 0.3% triton in PBS), 5% normal goat serum (Solarbio, China) in PBST (PBS containing 0.3% Triton X-100), primary antibody rabbit anti-c-Fos (1:2 000; 4 °C for 48 h), biotinylated goat anti-rabbit immunoglobulin G (IgG) (1:200; Vector Laboratories, USA), avidin-biotin peroxidase complex (1:200; ABC Kit; Vector Laboratories, USA), and chromogen solution consisting of 0.05% 3,3'-diaminobenzidine (Sigma-Aldrich, USA), 0.25% nickel ammonium sulfate (Sigma-Aldrich, USA), and 0.03% H_2O_2.

Transcriptome sequencing and data analysis

The brains used for RNA sequencing were removed from euthanized mice 24 h after ketamine injection, and the PFC was excised. The PFC samples from 12 lithium- and ketamine-treated mice were submitted to RNA extraction, RNA quantification, cDNA library preparation, and library quality assessment following standardized protocols by Novogene Co., Ltd. (China). After clustering and Illumina sequencing using the Illumina NovaSeq platform at Novogene, qualified sequences were aligned to the reference genome using Hisat2 v2.0.4. All downstream analyses were based on high-quality clean reads with Unique Molecular Identifiers. Differential expression analysis of the two groups was performed using the DESeq R package (v1.18.0). The resulting *P*-values were adjusted using the Benjamini and Hochberg approach for controlling the false discovery rate (FDR). Genes with an adjusted $P<0.05$ by DESeq were assigned as differentially expressed genes (DEGs). Gene Ontology (GO) enrichment analysis of the DEGs was implemented using the GOseq R package. GO terms with an adjusted $P<0.05$ were considered significantly enriched in DEGs. The Kyoto Encyclopedia of Genes and Genomes (KEGG) database allows analysis of high-level functions and utilities of biological systems, such as cells, organisms, and ecosystems, at the molecular level, especially large-scale molecular datasets generated by genome sequencing and other high-throughput technologies (http://www.genome.jp/kegg/). KOBAS was used to test statistical enrichment of the KEGG pathways in the DEGs.

Quantitative real-time PCR (qRT-PCR)

To validate the transcriptome sequencing data, 10 DEGs were randomly selected for verification by qRT-PCR, as described previously (Ding et al., 2021; Li et al., 2020; Ye et al., 2021; Zhang et al., 2021). Specific primers were designed according to reference sequences in the NCBI database with Primer-BLAST or PrimerBank and are listed in Table 1. The primers were synthesized by Sangon Biotech (China). Total RNA was extracted from the PFC using TRIzol reagent and reverse-transcribed into cDNA using HiScript III All-in-One RT SuperMix Perfect for qPCR Kit (Cat# R333, Vazyme, China). After reverse transcription, qRT-PCR was carried out on a QuantStudio™ 1 Applied Biosystem Real-Time PCR System (ThermoFisher Scientific, USA). The 20 μL reaction system contained 10 μL of PowerUp SYBR Green Master Mix (Cat. No. A25742; Applied Biosystems, USA), 0.5 μL of each primer (forward and reverse), 4 μL of cDNA template, and 5 μL of nuclease-free deionized water. The two-step method was performed for amplification with denaturation at 95 °C for 3 min, followed by 40 cycles at 95 °C for 5 s and 60 °C for 30 s; and final elongation at 95 °C for 15 s, 60 °C for 1 min, and 95 °C for 15 s. The relative mRNA expression levels of selected genes were calculated with the $2^{-\Delta\Delta Ct}$ method using

Table 1 Primer sequences used for qRT-PCR experiments

Items	Direction	Sequences
Hif3a	Forward primer	TACCTTATTCACCCCTCTTTGGA
	Reverse primer	AGCCAGGACAATTTTTCCGGT
Tcap	Forward primer	GATGCGCCTGGGTATCCTC
	Reverse primer	GATCGAGACAGGGTACGGC
Hspa8	Forward primer	TCTCGGCACCACCTACTCC
	Reverse primer	CTACGCCCGATCAGACGTTT
Iqgap2	Forward primer	TCCTCCAGACCAAACCTTCAT
	Reverse primer	TTGAGCAACAGGTATTCTTCCC
Thbs4	Forward primer	ACGGCTGAACAAAGCCATC
	Reverse primer	TTGCTCAGTCTCAGGAGAACC
Foxp2	Forward primer	AGTGTGCCCAATGTGGGAG
	Reverse primer	CATGATAGCCTGCCTTATGAGTG
Ciart	Forward primer	CTGAACGGACTCAAGATGGGT
	Reverse primer	ACCTCCTGAGGATGACTTCTG
Pla2g4e	Forward primer	ATGGTGACAGACTCCTTCGAG
	Reverse primer	CCTCTGCGTAAAGCTGTGG
Nptx2	Forward primer	TCAAGGACCGCTTGGAGAG
	Reverse primer	CGAGGTCTCATTATGAAGCAGG
Maml3	Forward primer	GCATCCCACACAACCAATCC
	Reverse primer	TGCGAGAGAGCCGAGTTCA
Gapdh	Forward primer	AGGTCGGTGTGAACGGATTTG
	Reverse primer	GGGGTCGTTGATGGCAACA

GAPDH as an internal reference. Each sample was tested in duplicate.

Western blot analysis

Western blotting was performed following previous protocols of our laboratory (Ni et al., 2018). Tissues were homogenized with a TGrinder Tissue Homogenizer (Tiangen Biotechnologies, China) in cold denaturing buffer from the Minute™ Total Protein Extraction Kit (SD-001, Invent Biotechnologies, USA), protease inhibitor cocktail (Sigma-Aldrich, USA), and phosphatase inhibitor cocktail II (Sigma-Aldrich, USA). Tissue homogenates were centrifuged at 15 000 r/min and 4 °C for 15 min to clear cellular debris. Cultured cells were harvested and lysed in cold denaturing buffer from the Minute™ Total Protein Extraction Kit (SD-001, Invent Biotechnologies, USA), protease inhibitor cocktail (Sigma-Aldrich, USA), and phosphatase inhibitor cocktail II (Sigma-Aldrich). Total protein was measured using a Pierce BCA Protein Assay Kit (Thermo Fisher Scientific, USA). The supernatant was then mixed with 5×loading buffer (Sangon Biotech, China) and boiled for 10 min. The protein sample was run on an 8% sodium dodecyl sulfate (SDS) polyacrylamide gel (120 V, 1 h), then transferred to a polyvinylidene fluoride membrane (Millipore, USA) using a constant current of 300 mA for 2.5 h at 4 °C. Membranes were blocked for 1 h at 37 °C in PBS-tween buffer (0.01 mol/L PBS and 0.05% Tween-20) containing 5% non-fat milk and incubated for 2 h at room temperature with primary antibodies monoclonal mouse anti-FLAG (1 : 2 000; #F1804; Sigma-Aldrich, USA) and mouse anti-GAPDH (1 : 3 000; sc-32233; Santa Cruz Biotechnology, USA) diluted in PBS-tween buffer with 0.5% non-fat milk. The membranes were then incubated at 4 °C overnight. After washing, the membranes were incubated for 1.5 h at room temperature with anti-mouse-horseradish peroxidase (HRP) (1:2 000; sc-2005; Santa Cruz Biotechnology, USA). After rinsing, subsequent detection was performed using the ECL Western Blot System (SuperSignal West Pico Chemiluminescent Substrate, Pierce, USA). Immunoreactive bands were recorded using the ChemiDoc Touch Imaging System (Bio-Rad Laboratories, USA).

Digital photomicrographs and data quantification

Representative images of the PFC sections were taken using a whole slide scanner (Nanozoomer XR, Hamamatsu, Japan). To count the c-Fos-immunoreactive (c-Fos-ir) cells, ImageJ v1.46r (National Institutes of Health, USA) software was used to select the mPFC and count c-Fos-ir nuclei, as described previously (Gao et al., 2021). According to previous studies, a 150 μm interval between adjacent sections was used to avoid oversampling the same c-Fos-ir cells (Coggeshall & Lekan, 1996; Ni et al., 2020b). An observer blind to group assignment analyzed the sample sections at 200× magnification. The c-Fos-ir nuclear profiles (solid round or oval shaped) should be larger than 4 μm in diameter. In ImageJ, a random grid was applied to each image with an area of 200 μm^2. Nuclear profile density was measured based on the number of positive cells per mm^2 in each grid.

Statistical analysis

All data are presented as means±standard error of the mean (*SEM*), and no data were excluded. Significant differences were determined using two-way analysis of variance (ANOVA) and Fisher's LSD *post hoc* test for comparison with SPSS v25 software (SPSS Inc., USA). For non-normally distributed data, latency to open arms and frequency of entries into the central area and open arms of the maze were compared using the Kruskal-Wallis *H* test with Bonferroni correction in pairwise analyses. Repeated measures ANOVA followed by Bonferroni's *post hoc* test was also used to evaluate the significance of distance moved and cumulative duration in the OFT every 1 min or 5 min. For comparisons between more than two groups, the chi-square test was used to analyze whether the percentage of mice that fell off the platform differed significantly among groups, followed by pairwise comparisons with Fisher's exact test (using α correction) to determine which groups were significantly different. Unpaired *t*-test was used to compare the means between two groups. A probability value of $P<0.05$ was considered statistically significant in all cases. Histograms were plotted using GraphPad Prism (GraphPad Software, USA).

RESULTS

Chronic lithium exposure attenuated ketamine-induced mania-like behavior

To determine whether ketamine-induced mania-like behavior is sensitive to chronic lithium treatment, we injected (i.p.) mice with lithium or saline for 8 days, followed by a single dose of ketamine (Figure 1A). Acute ketamine treatment markedly increased locomotor activity in the first 25 min after injection (Figure 1B). However, this effect was partially reversed by chronic lithium exposure (Figure 1B; $F(3, 44)=15.900$, $P<0.01$). A single dose of ketamine significantly increased the total distance moved and cumulative duration of immobility (velocity<1.75 cm/s) during the 75 min open-field session, while pretreatment with chronic lithium for 8 days significantly reversed these changes (Figure 1C; lithium pretreatment: ($F(1, 44)=10.322$, $P<0.01$), ketamine treatment: ($F(1, 44)=41.798$, $P<0.01$), lithium×ketamine interaction: ($F(1, 44)=7.863$, $P<0.01$); Figure 1D; lithium pretreatment: ($F(1, 44)=8.109$, $P<0.01$), ketamine treatment: ($F(1, 44)=22.645$, $P<0.01$), lithium×ketamine interaction: ($F(1, 44)=9.353$, $P<0.01$)). In the EPM test, no saline- or lithium-treated mice fell off the platform. However, 76.47% (13/17) of ketamine-treated mice fell off the platform, which declined to 33.33% (6/18) of ketamine-treated mice under lithium pretreatment (Figure 1E; $P<0.001$, Fisher's exact test). In addition, ketamine administration reduced the latency to fall off the open arms (Figure 1F; Kruskal-Wallis *H* test, $H=34.009$, $P<0.001$) and the latency to open arms in each group (Figure 1I; Kruskal-Wallis *H* test, $H=12.372$, $P<0.01$) and increased the cumulative duration of movement (velocity> 1.75 cm/s; Figure 1G; two-way ANOVA, $P<0.05$) and time spent in the open arms (Figure 1H; Kruskal-Wallis *H* test, $H=33.541$, $P<0.01$). Chronic lithium exposure partially attenuated these ketamine-induced behavioral changes (Figure 1F-I).

Chronic lithium exposure reversed ketamine-induced c-Fos expression in the mPFC

We determined the quantitative expression of c-Fos immunoreactivity in the mPFC of adult male mice in the saline/saline-, lithium/saline-, saline/ketamine-, and lithium/ketamine-treated groups (Figure 1J–N). Two-way ANOVA revealed that the significant increase in c-Fos expression induced by a single injection of ketamine was blocked by chronic lithium administration for 8 days in the medial orbital cortex (MO; Figure 1K; lithium pretreatment: (F(1, 20)=3.368, P>0.05), ketamine treatment: (F(1, 20)=6.793, P<0.05), lithium×ketamine interaction: (F(1, 20)=11.901, P<0.01)), infralimbic cortex (IL; Figure 1L; lithium pretreatment: (F(1, 22)=3.309, P>0.05), ketamine treatment: (F(1, 20)=7.522, P<0.05), lithium×ketamine interaction: (F(1, 20)=6.060, P<0.05)), and prelimbic cortex (PrL; Figure 1M; lithium pretreatment: (F(1, 20)=4.320, P>0.05), ketamine treatment: (F(1, 20)=10.964, P<0.01), lithium×ketamine interaction: (F(1, 20)=13.736, P<0.01)). In the PrL, sparse c-Fos-ir cells were observed in the saline/saline-, lithium/saline-, and lithium/ketamine-treated mice, whereas a high density of c-Fos-ir cell nuclei was found in the saline/ketamine-treated mice (Figure 1N).

Effects of lithium on ketamine-induced transcriptome in the PFC

To identify potential drug targets for the lithium- and/or ketamine-treated mice, we analyzed global gene expression in the PFC of the saline/saline-, saline/ketamine-, and lithium/ketamine-treated mice by transcriptome sequencing (RNA sequencing). In total, 235 DEGs were identified in the PFC of the saline/ketamine-treated mice (P-adjusted<0.05, $|\log_2(\text{fold-change})|>1$) compared to the saline/saline-treated mice (Figure 2A). Of these genes, 202 were up-regulated and 33 were down-regulated (Figure 2A). In addition, 448 genes were identified in the saline/ketamine-treated vs. lithium/ketamine-treated mice, including 207 up-regulated and 241 down-regulated genes (Figure 2B). We also conducted hierarchical cluster analysis of DEGs among samples from the saline/saline-, saline/ketamine-, and lithium/ketamine-treated mice (Figure 2C). The identified DEGs were grouped into four clusters. To identify common DEGs among groups, we generated a Venn diagram showing the overlap of four significant targets (Figure 2D). Moreover, GO analysis of the DEGs (Figure 2E-F) identified many significantly enriched GO terms in the saline/ketamine-treated vs. lithium/ketamine-treated mice (Figure 2F). Furthermore, 20 significantly enriched KEGG pathways were identified (Figure 2G, H), with the Notch signaling pathway and circadian rhythm found to be the top significantly enriched pathways. Interestingly, the top enriched genes were involved in the PI3K-AKT signaling pathway among all pairwise comparisons (seven and 17 genes in Figure 2G and H, respectively). The location of these enriched genes is shown in the simplified PI3K-AKT signaling pathway (Figure 3A, B). Results showed that 71.4% (5 of 7) of the enriched DEGs in the PI3K-AKT signaling pathway were up-regulated in the saline/saline-treated vs. saline/ketamine-treated mice, while 64.7% (11 of 17) were down-regulated in the saline/ketamine-treated vs. lithium/ketamine-treated mice (Figure 3A, B).

To verify the reliability of the DEGs obtained from RNA sequencing, we randomly selected 10 genes (*Pla2g4e*, *Iqgap2*, *Maml3*, *Ciart*, *Hspa8*, *Hif3a*, *Nptx2*, *Tcap*, *Foxp2*, and *Thbs4*) for qRT-PCR (Figure 3C). The results were nearly consistent with the RNA sequencing trends, indicating that our transcriptome sequencing analysis was accurate and reliable.

Inhibition of AKT reversed ketamine-induced mania-like behavior

To determine the role of AKT in the mPFC in the development of mania-like behavior, we tested the effects of AKT-shRNA, used to selectively knockdown AKT, on ketamine-induced mania-like behavior in mice (Figure 4A). Knockdown efficiency of AKT-shRNA was initially demonstrated by western blot analysis (Figure 4C). The AKT-shRNA and control shRNA viruses were injected into the bilateral mPFC of male mice at 8 weeks of age through the pre-implanted cannulas (Figure 4B). After surgery, the mice were allowed to recover and express the virus for 3 weeks before the behavioral experiments were performed (Figure 4D). Mice treated with AKT-shRNA gained significantly more body weight compared to the control mice (Figure 4E; t_{27}=–2.195, P<0.05). In addition, the ketamine-treated mice treated with AKT-shRNA displayed a lower frequency of entries into the central area (Figure 4F; AKT-shRNA pretreatment: (F(1, 24)=1.847, P>0.05), ketamine treatment: (F(1, 24)=13.997, P<0.01), AKT-shRNA×ketamine interaction: (F(1, 24)=5.330, P<0.05)) and less time spent in the central area (Figure 4G; F(3, 24)=8.032, P<0.01; Figure 4H, I; F(3, 24)=8.723, P<0.001) during the 10 min OFT than the ketamine-treated mice treated with the control shRNA.

To further test whether the PI3K-AKT signaling pathway is responsible for mania-like behavior in ketamine-treated mice, we analyzed the effects of AKT signaling inhibition by MK2206, a selective AKT inhibitor (Figure 5A). Male mice received MK2206 or vehicle once/day for three consecutive days. The behavioral tests were performed at 60 min after the third administration of MK2206 and completed within 30 min of the single administration of ketamine. In the 10 min OFT, MK2206 treatment significantly decreased total distance traveled (Figure 5B, C; MK2206 pretreatment: (F(1, 24)= 202.706, P<0.001), ketamine treatment: (F(1, 24)=33.624, P<0.001), MK2206×ketamine interaction: (F(1, 24)=19.871, P<0.001); Figure 5D; F(3, 24)=85.400, P<0.001) and time spent in the central area (Figure 5F; F(3, 24)=6.136, P<0.01) compared to ketamine-treated mice receiving the vehicle treatment. Moreover, treatment with MK2206 significantly increased the total cumulative duration of immobility (velocity<1.75 cm/s) in the ketamine-treated mice (Figure 5E; MK2206 pretreatment: (F(1, 24)=141.559, P<0.001), ketamine treatment: (F(1, 24)=24.272, P<0.001), MK2206×ketamine interaction: (F(1, 24)=7.368, P<0.05)). In the 5 min EPM test, the ketamine-treated mice administered three injections of MK2206 (40 mg/kg) showed a significant decrease in total distance traveled (Figure 5G; MK2206 pretreatment: (F(1, 24)=72.954, P<0.001), ketamine treatment: (F(1, 24)=12.862, P<0.01), MK2206×ketamine interaction: (F(1, 24)=6.137, P<0.05)) and time spent in the open arms (Figure 5I; F(3,

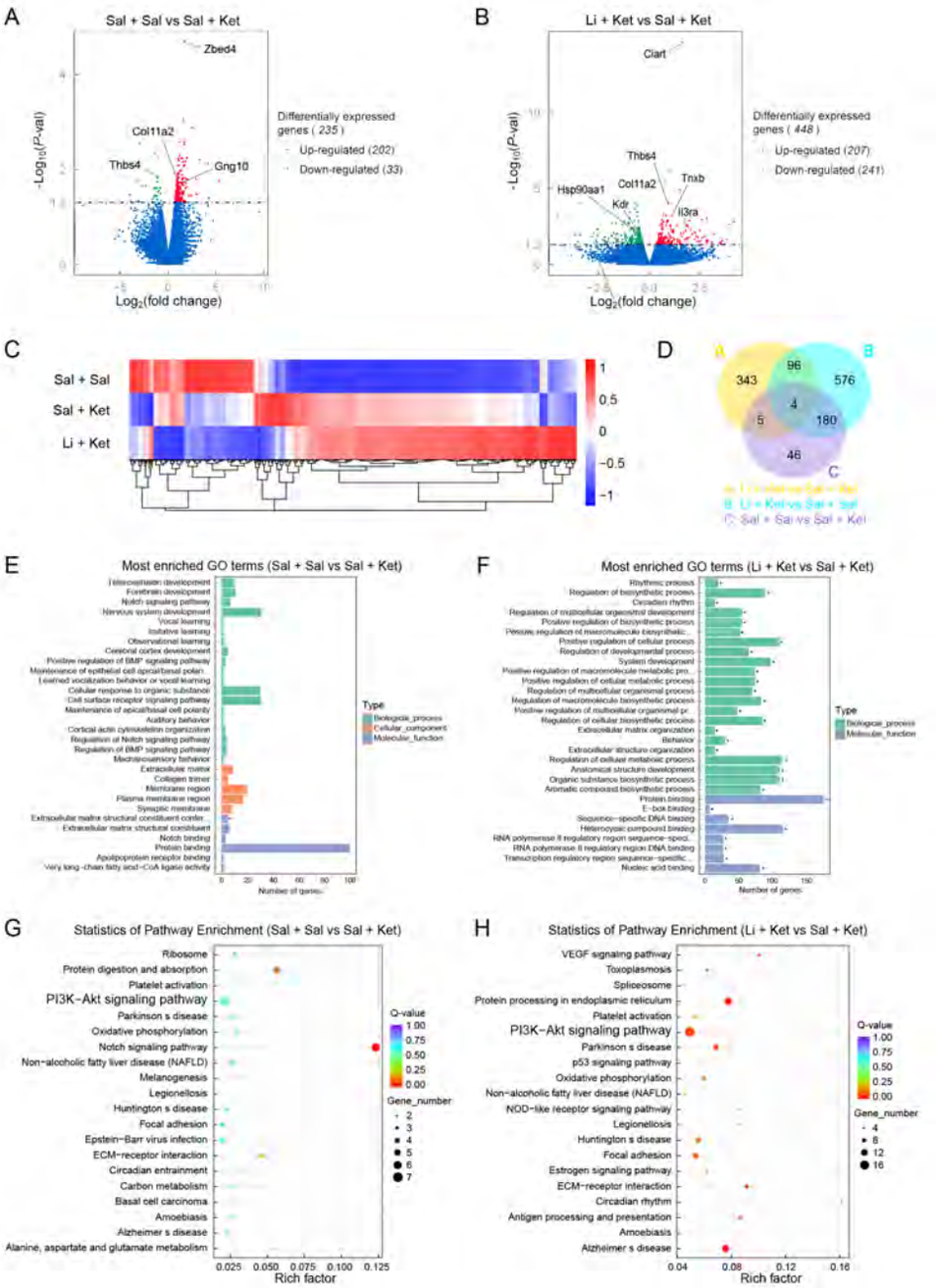

Figure 2 Effects of lithium on ketamine-induced transcriptome in the PFC

A: Volcano plot of DEGs in the PFC between Sal+Sal and Sal+Ket groups (*n*=4, each group). Red dots represent genes with up-regulated expression, green dots represent genes with down-regulated expression, and blue dots represent non-DEGs. Labels are given as gene symbols for the top genes by unadjusted *P*-value rank (Zbed4), top three genes were enriched in the PI3K-AKT signaling pathway. B: Volcano plot of DEGs in the PFC between Sal+Ket and Li+Ket groups (*n*=4, each group). Labels are given as gene symbols for the top genes by unadjusted *P*-value rank (Ciart), top six genes were enriched in the PI3K-AKT signaling pathway. C: Hierarchical cluster analysis of DEGs among samples in the Sal+Sal, Sal+Ket, and Li+Ket groups (red, up-regulated; blue, down-regulated). D: Venn diagram showing distribution of DEGs among the three groups. E: Top 30 significantly enriched GO categories of biological process, cellular component, and molecular function terms between Sal+Sal and Sal+Ket groups. X-axis indicates number of DEGs. Y-axis indicates GO terms. Asterisks represent significant differences. F: Top 30 significantly enriched GO categories of biological process and molecular function terms between Sal+Ket and Li+Ket groups. G: Scatter plots showing top 20 enriched KEGG pathways between the Sal+Sal and Sal+Ket groups. Y-axis indicates KEGG pathways. X-axis indicates Rich factor (i.e., ratio of the number of DEGs annotated in this pathway term to the number of all genes annotated in this pathway term). The *Q*-value is a corrected *P*-value ranging from 0 to 1. Size and color of the bubble represent number of DEGs and significance of enrichment in the pathway. H: Scatter plots showing top 20 enriched KEGG pathways between Sal+Ket and Li+Ket groups. Ket, ketamine; Li, lithium; Sal, saline.

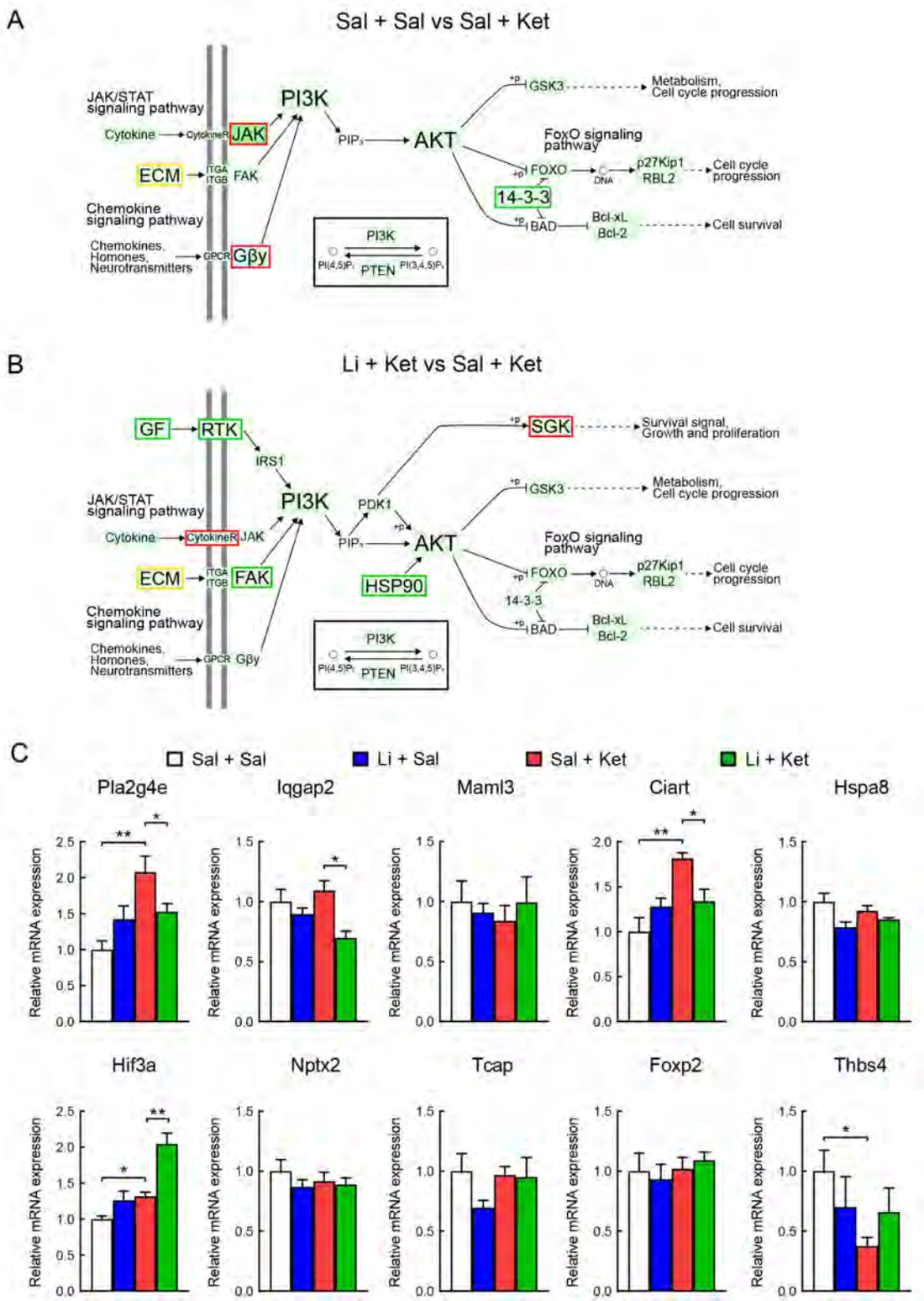

Figure 3 Simplified PI3K-AKT signaling pathway showing location of significant genes based on KEGG pathway enrichment analysis

A: Enriched PI3K-AKT signaling pathway between Sal+Sal and Sal+Ket groups. Red frame genes represent up-regulated DEGs, green frame genes represent down-regulated DEGs, and yellow frame genes represent DEGs with up-regulated and down-regulated expression. B: Enriched PI3K-AKT signaling pathway between Sal+Ket and Li+Ket groups. C: Validation of DEG expression by qRT-PCR (n=5, each group). Ket, ketamine; Li, lithium; Sal, saline. *: P<0.05; **: P<0.01.

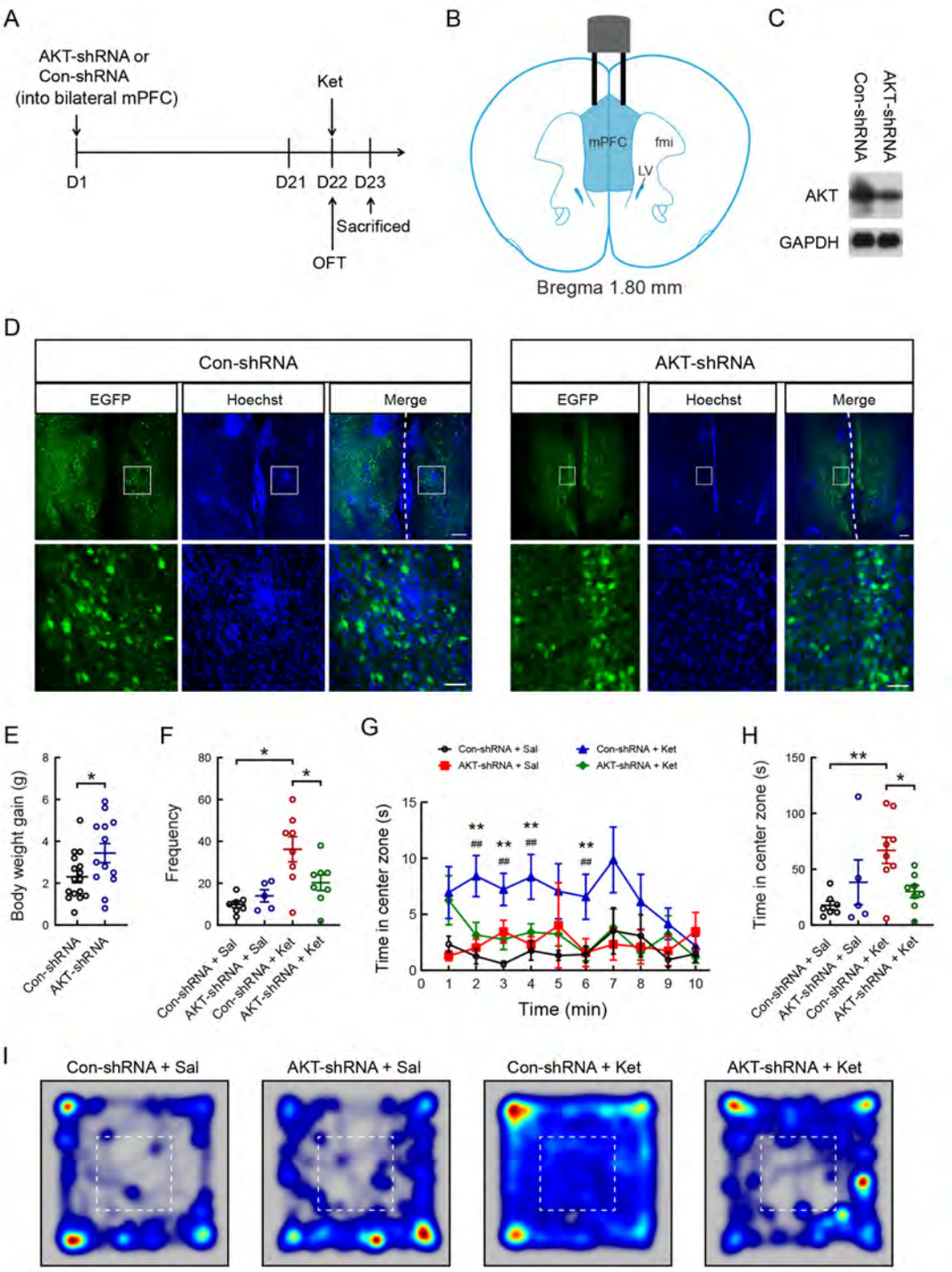

Figure 4 Effects of selective AKT knockdown by AKT-shRNA on ketamine-induced mania-like behavior in mice

A: Timeline of the experiment. B: Localization of guide cannula tips in the mPFC of mice. C: Western blot analysis demonstrated the knockdown efficiency of AKT-shRNA in 293T cells using AAV-AKT-shRNA-EGFP. D: Fluorescence microscopy images showing transfection efficiency of AKT-shRNA and control shRNA in mouse mPFC (green). Top row: low-magnification images illustrating EGFP- and Hoechst-labeled cells in the mPFC (shaded area in b, dotted lines delineate medial boundary of the cerebral hemisphere); bottom row: high-magnification images showing EGFP- and Hoechst-labeled cells (boxed areas in top row). E: Body weight gain following treatment with AKT-shRNA and control shRNA. F: Frequency of entry into central area during 10 min OFT in each group. G: Time in central area in 1 min bins for each group. Con-shRNA+Sal vs. Con-shRNA+Ket: **: P<0.01; AKT-shRNA+Ket vs. Con-shRNA+Ket: $^{\#\#}$: P<0.01. H: Total time spent in central area in OFT. I: Representative heatmaps showing cumulative duration spent by each group throughout the compartment during 10 min OFT. Dashed lines represent central areas. Con-shRNA, control shRNA; Ket, ketamine; Sal, saline. *: P<0.05; **: P<0.01 (n=7–8, each group).

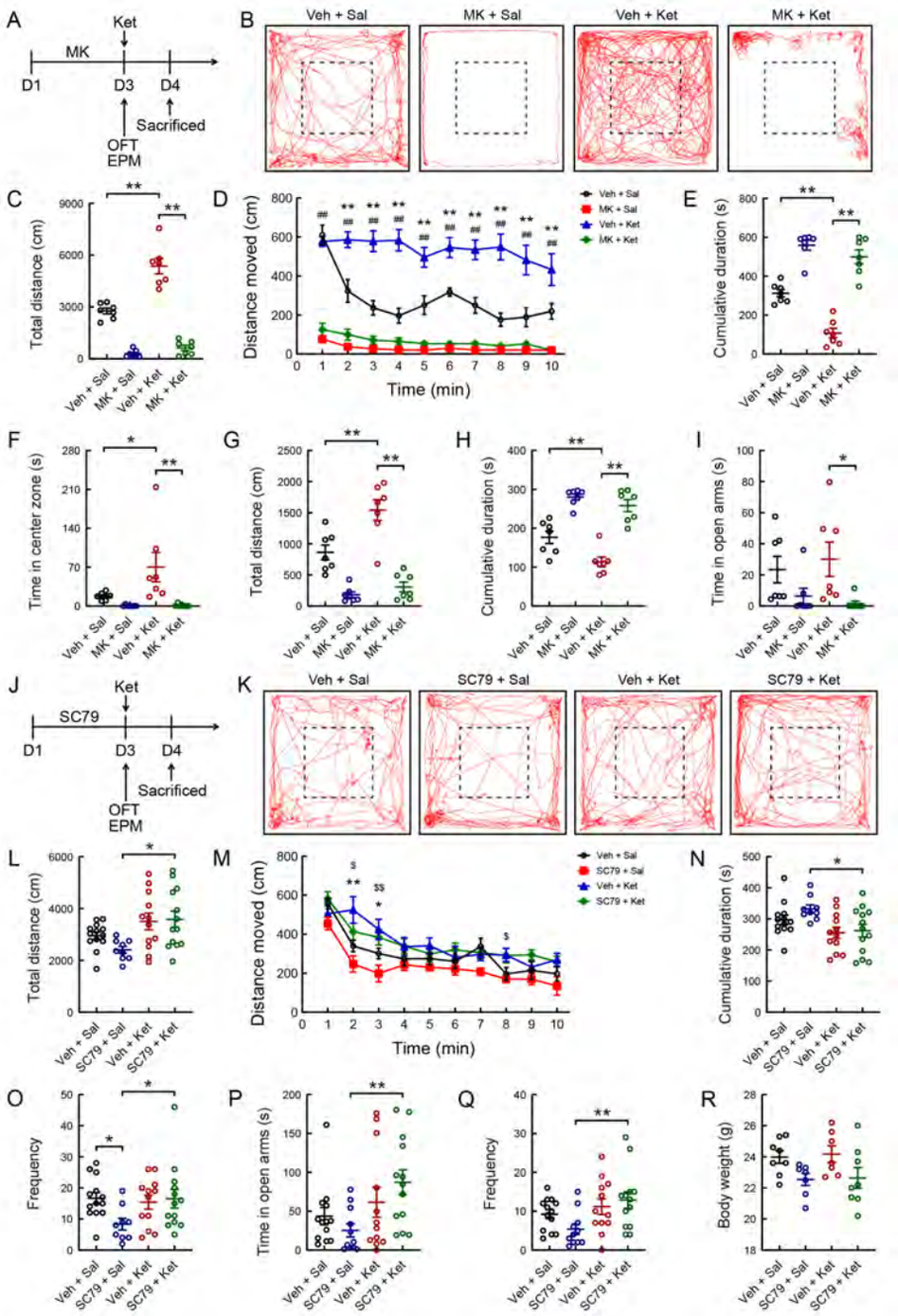

Figure 5 Effects of MK2206 (selective AKT inhibitor) and SC79 (AKT activator) on mania-like behavior in mice

A: Timeline of the experiment. B: Representative traces of mouse movement (red lines) in each group during 10 min OFT. Dotted lines delineate center area. C: Total distance moved during 10 min OFT. D: Distance traveled in 1 min bins for each group (n=7, each group). Veh+Sal vs. Veh+Ket: **: P<0.01; MK+Ket vs. Veh+Ket: $^{\#\#}$: P<0.01. E: Total cumulative duration of not moving (velocity<1.75 cm/s). F: Time in center area during 10 min OFT. G: Total distance moved during 5 min EPM test in each group. H: Total cumulative duration of immobility (velocity<1.75 cm/s) in EPM test. I: Time spent in open arms during 5 min EPM test. J: Timeline of the experiment. K: Representative traces of mouse movement (red lines) in each group (n=12–13, each group) during 10 min OFT. Dotted lines delineate center area. L: Total distance moved during 10 min OFT. M: Distance traveled in 1 min bins in open field. Veh+Sal vs. Veh+Ket: *: P<0.05, **: P<0.01; SC79+Ket vs. SC79+Sal: $^{\$}$: P<0.05, $^{\$\$}$: P<0.01. N: Total cumulative duration of immobility (velocity<1.75 cm/s). O: Frequency of entry into central area during 10 min OFT in each group. P: Time spent in open arms during 5 min EPM test. Q: Frequency of entry into open arms of maze. R: Body weight following treatment with SC79 and ketamine. Ket, ketamine; MK, MK2206; Sal, saline; Veh, vehicle. *: P<0.05; **: P<0.01.

24)=3.303, P<0.05). Additionally, the total cumulative duration of immobility was significantly increased in the MK2206- and ketamine-treated mice compared to the ketamine-treated mice (Figure 5H; F(3, 24)=33.115, P<0.001).

Activation of AKT contributed to mania-like behavior in low-dose ketamine-treated mice

To determine whether activation of the AKT signaling pathway is required for mania-like behavior development in ketamine-treated mice, we examined the effects of SC79, an AKT activator, on behaviors induced by low-dose ketamine (5 mg/kg) in mice (Figure 5J). Mice were treated with SC79 (40 mg/kg) or vehicle daily for three consecutive days. The following behavioral tests were conducted 60 min after the third administration of SC79 and completed within 30 min of the single administration of ketamine (Figure 5J). Compared to the SC79-treated mice, administration of ketamine in the SC79-treated mice markedly increased the total distance traveled (Figure 5K, L; Kruskal-Wallis H test, H=9.678, P<0.05) and frequency of entries into the center (Figure 5O; Kruskal-Wallis H test, H=7.904, P<0.05) in the OFT. The distance traveled in 1 min bins throughout the 10 min OFT was measured (Figure 5M; F(3, 43)=3.784, P<0.05). Two-way ANOVA revealed significant differences in the total cumulative duration of immobility (Figure 5N; F(3, 43)=3.592, P<0.05). Moreover, single low-dose ketamine treatment significantly increased the time spent in the open arms (Figure 5P; Kruskal-Wallis H test, H=10.321, P<0.05) and the frequency of entries into the open arms of the maze (Figure 5Q; Kruskal-Wallis H test, H=9.339, P<0.05) in the SC79-treated mice but not in the vehicle-treated mice. No differences in body weight were observed among the four groups (Figure 5R).

Inhibition of PI3K reversed ketamine-induced mania-like behavior

To investigate whether PI3K is required for ketamine-induced mania-like behavior, we used LY294002, a specific PI3K inhibitor (Figure 6A). Naive mice received an i.p. injection of LY294002 (25 mg/kg) and vehicle daily for two consecutive days, and the OFT was performed 60 min after the second administration (Figure 6A). LY294002 treatment significantly inhibited the total distance traveled (Figure 6B, C; F(3, 28)=16.194, P<0.001; Figure 6D; F(3, 28)=18.068, P<0.001) and frequency of entries into the central area (Figure 6F; Kruskal-Wallis H test, H=16.449, P<0.01) in the ketamine-treated mice compared to the vehicle injection. In addition, treatment with LY294002 significantly increased the total cumulative duration of immobility compared with the vehicle treatment in the ketamine-treated mice (Figure 6E; Kruskal-Wallis H test, H=20.969, P<0.001).

Inhibition of mTOR had no effect on ketamine-induced mania-like behavior

To examine whether the mTOR signaling pathway is required for ketamine-induced mania-like behavior, we treated mice with rapamycin, a specific mTOR inhibitor (Figure 6G). Male mice were administered rapamycin (10 mg/kg) or vehicle once/day for 3 days (Figure 6G). Two-way ANOVA revealed that ketamine administration significantly increased the total distance moved (Figure 6H–J), time spent in the central area (Figure 6K), and frequency of entries into the central area (Figure 6L) compared with the control group, and these effects were not reversed by rapamycin pretreatment.

DISCUSSION

In the present study, we found that chronic lithium exposure attenuated ketamine-induced mania-like behavior and c-Fos expression in the mPFC of adult male mice. Furthermore, to determine the effects of lithium administration in ketamine-treated mice on the PFC transcriptome, RNA sequencing confirmed the inactivation of the PI3K-AKT signaling pathway. Inhibition of the PI3K-AKT signaling pathway by pharmacological and genetic manipulation reversed ketamine-induced mania-like behavior. However, inhibition of mTOR had no effect on ketamine-induced mania-like behavior. Importantly, activation of the PI3K-AKT signaling pathway contributed to mania-like behavior in low-dose ketamine-treated mice.

Numerous studies have supported the dose-dependent effects of ketamine on rodent behavior (Radford et al., 2017; Wu et al., 2020). Low-dose ketamine (10 mg/kg) shows antidepressant activity in rodents via its metabolites, which activate AMPAR (Qin et al., 2021; Zhou et al., 2014). In contrast, high doses of sub-anesthetic and anesthetic ketamine (>40 mg/kg) produce long-lasting psychotomimetic phenotypes by activating NMDAR and brain-derived neurotrophic factor (BDNF) (Qin et al., 2021; Wu et al., 2020). Moderate doses of ketamine (20–30 mg/kg) can also induce hyperactivity and manic behaviors in mice (Acevedo & Siegel, 2022; Gao et al., 2021; Openshaw et al., 2020).

Acute and repeated exposure to ketamine in rodents can mimic aspects of manic episodes in BD patients (Hu et al., 2021; Nichols et al., 2016; Ricke et al., 2011). In this study, acute ketamine exposure in mice induced mania-like behavior, consistent with previous findings in mice (Gao et al., 2021) and rats (Ettenberg et al., 2020; Ghedim et al., 2012; Krug et al., 2019). Chronic lithium administration is the gold-standard treatment for BD and can attenuate ketamine-induced mania-like behavior in male mice (Gao et al., 2021) and rats (Krug et al., 2019), as shown in our study. Acute ketamine treatment can also increase c-Fos expression (an indicator of increased neuronal activity) in the lateral septal nucleus, hypothalamus, amygdala, and hippocampus of male mice (Gao et al., 2021). Consistently, our findings showed that the mPFC was activated by a single dose of ketamine. Interestingly, lithium moderated the effects of single-dose ketamine on c-Fos expression in the mPFC. Clinical studies have found abnormal activity in the PFC of BD patients (Bjertrup et al., 2022; Chai et al., 2011; Yang et al., 2020) and documented the neuroprotective effects of lithium on the PFC in BD patients (Altinay et al., 2018; Hajek et al., 2012).

This study is the first to illustrate the transcriptional programs in the PFC activated in response to lithium administration in ketamine-treated mice. At the transcriptional level, our data demonstrated the presence of common enriched pathways between the saline/saline-treated vs. saline/ketamine-treated mice and the saline/ketamine-treated vs. lithium/ketamine-treated mice. KEGG pathway analysis

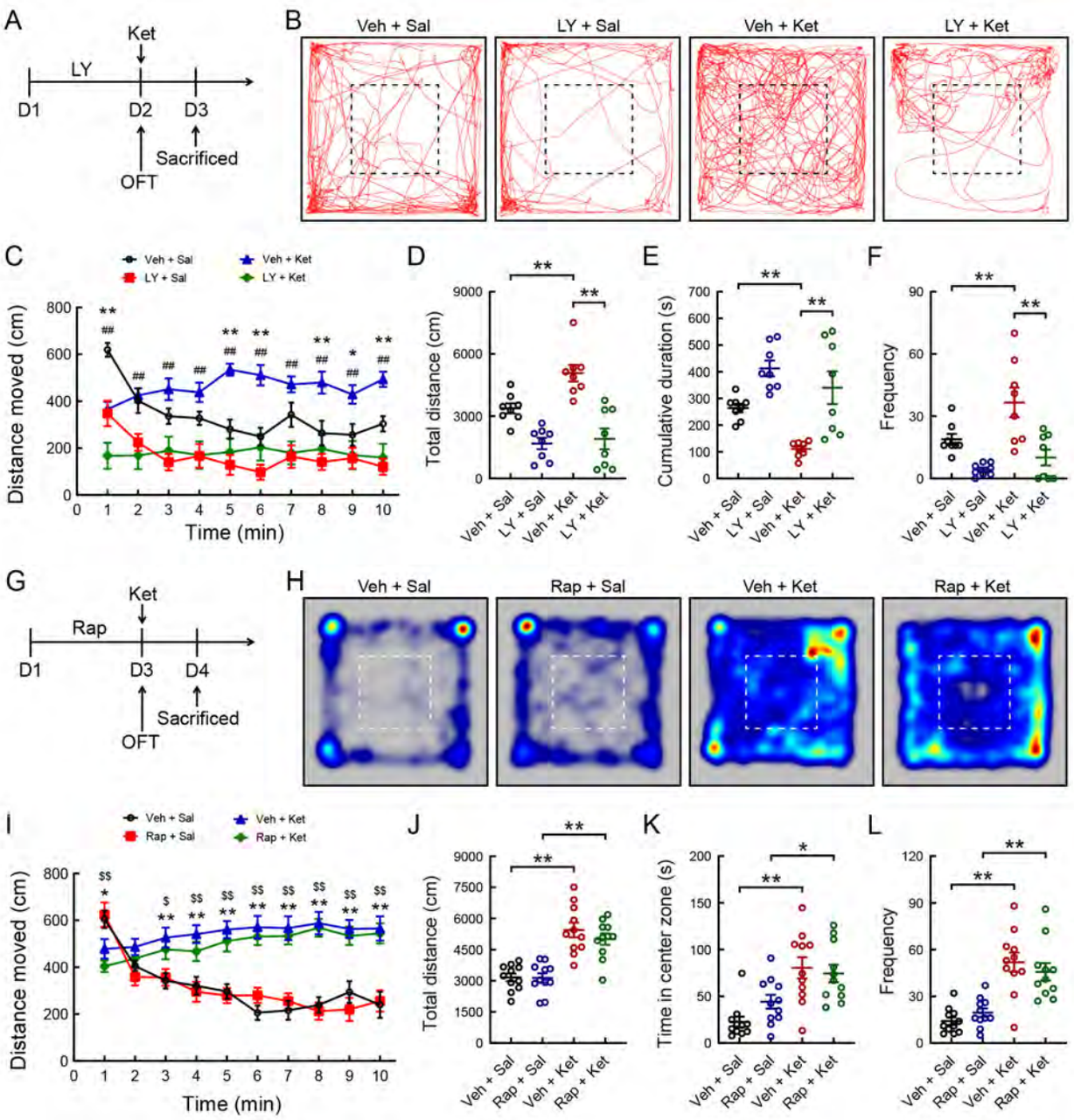

Figure 6 Effects of LY294002 (specific PI3K inhibitor) and rapamycin (specific mTOR inhibitor) on ketamine-induced mania-like behavior in mice

A: Timeline of the experiment. B: Representative traces of mouse movement (red lines) in each group (*n*=8, each group) during 10 min OFT. Dotted lines delineate center area. C: Distance moved in 1 min bins for each group. Veh+Sal vs. Veh+Ket: *: P<0.05, **: P<0.01; LY+Ket vs. Veh+Ket: $^{\#\#}$: P<0.01. D: Total distance moved during 10 min OFT. E: Total cumulative duration of not moving (velocity<1.75 cm/s) in open field. F: Frequency of entry into central area during 10 min OFT in each group. G: Timeline of the experiment. H: Representative heatmaps showing cumulative duration spent by each group (*n*=11, each group) throughout the compartment during 10 min OFT. Dashed lines represent central areas. I: Distance moved in 1 min bins for each group. Veh+Sal vs. Veh+Ket: *: P<0.05, **: P<0.01; Rap+Ket vs. Rap+Sal: $^{\$}$: P<0.05, $^{\$\$}$: P<0.01. J: Total distance moved during 10 min OFT. K: Total time spent in central area in OFT. L: Frequency of entry into central area during 10 min OFT in each group. Ket, ketamine; LY, LY294002; Rap, rapamycin; Sal, saline; Veh, vehicle. *: P<0.05; **: P<0.01.

indicated that the top enriched genes in the three groups were involved in the PI3K-AKT signaling pathway. Consistently, changes in the AKT signaling pathway have been reported in the whole blood (Machado-Vieira et al., 2015) and PFC of BD patients (Vanderplow et al., 2021). Chronic ketamine exposure produces a resilient phenotype mediated by changes in the

AKT signaling pathway and neuronal activity in the brains of adolescent mice (Parise et al., 2021). In addition, lithium exerts its neuroprotective activity via the PI3K-AKT signaling pathway (Ates et al., 2022; Pan et al., 2011). GSK-3beta, presumably through the AKT signaling pathway, mediates the hyperlocomotion-suppressing effects of lithium in rodent models of mania (Urs et al., 2012; Valvassori et al., 2017). These findings demonstrate that the PI3K-AKT signaling pathway, as a common signaling pathway for ketamine and lithium, plays a critical role in mania-like behaviors.

To determine whether the PI3K-AKT signaling pathway is responsible for mania-like behavior in ketamine-treated mice, we used pharmacological and genetic manipulations to specifically alter AKT and PI3K and investigate behavioral changes in ketamine-treated mice. We first demonstrated that selective AKT knockdown by viral delivery of AKT-shRNA in the mPFC reversed ketamine-induced mania-like behavior in mice. Recent research has indicated that viral-mediated down-regulation of AKT expression in the ventral tegmental area blocks the effects of repeated ketamine treatment on chronic social defeat stress-induced behavioral deficits in mice (Parise et al., 2021). Moreover, the selective AKT inhibitor MK2206 produced anti-manic effects in ketamine-treated mice in our study. Experimental evidence suggests that low-dose ketamine administration has no effect on locomotor activity in mice (Akillioglu et al., 2012; Aleksandrova et al., 2020; Khakpai et al., 2019). Intriguingly, we found that low-dose ketamine itself could not effectively induce mania, but significant effects were observed when combined with the AKT activator SC79. However, further study is required to determine whether low-dose ketamine induces mania-like behavior in AKT-overexpressing transgenic mice. Exposure to the specific PI3K inhibitor LY294002 is reported to inhibit locomotor activity during the OFT (Shin et al., 2021; Xing et al., 2019). Our data also confirmed that LY294002 significantly decreased locomotor activity in mice. Importantly, inhibition of PI3K also reversed ketamine-induced mania-like behavior. However, the specific mTOR inhibitor rapamycin did not inhibit locomotor activity in the OFT in naive controls, consistent with previous research (Hadamitzky et al., 2018; Xing et al., 2019), and inhibition of mTOR had no effect on locomotor activity in the saline-treated mice or on mania-like behavior in the ketamine-treated mice. Thus, our experimental findings suggest that PI3K and AKT, but not mTOR, may be novel therapeutic targets for treating mania. However, our study is not without limitations and further research is required to investigate the signaling mechanism downstream of PI3K-AKT signaling molecules.

In conclusion, chronic lithium exposure attenuated mania-like behavior in ketamine-treated mice via the PI3K-AKT signaling pathway in the mPFC. Inhibition of the PI3K-AKT signaling pathway rescued ketamine-induced mania-like behavior. Our study thus identified PI3K-AKT signaling as a new therapeutic target for BD.

DATA AVAILABILITY

Raw data were deposited in the National Center for Biotechnology Information database under BioProjectID PRJCA012231, Genome Sequence Archive under Accession No. CRA008352, and Science Data Bank under DOI: 10.57760/sciencedb.03000.

COMPETING INTERESTS

The authors declare that they have no competing interests.

AUTHORS' CONTRIBUTIONS

R.J.N. was involved in apparatus design, behavioral tests, data interpretation, and manuscript writing. T.H.G., Y.Y.W., and Y.T. were involved in apparatus design and behavioral tests. J.X.W., L.S.Z., and P.N. were involved in data analyses. X.H.M. and T.L. were responsible for experimental design and revision of the manuscript. All authors read and approved the final version of the manuscript.

ACKNOWLEDGEMENTS

We would like to thank Qi-Qi Zhou and Hong Bu (Institute of Clinical Pathology, West China Hospital of Sichuan University, Chengdu, China) for microscopic observations.

REFERENCES

Acevedo J, Siegel JA. 2022. Neurobiological, behavioral, and cognitive effects of ketamine in adolescents: a review of human and pre-clinical research. *Behavioural Brain Research*, **435**: 114049.

Akillioglu K, Melik EB, Melik E, Boga A. 2012. Effect of ketamine on exploratory behaviour in BALB/C and C57BL/6 mice. *Pharmacology Biochemistry and Behavior*, **100**(3): 513−517.

Aleksandrova LR, Wang YT, Phillips AG. 2020. Ketamine and its metabolite, (2R, 6R)-HNK, restore hippocampal LTP and long-term spatial memory in the Wistar-Kyoto rat model of depression. *Molecular Brain*, **13**(1): 92.

Alonso J, Petukhova M, Vilagut G, Chatterji S, Heeringa S, Üstün TB, et al. 2011. Days out of role due to common physical and mental conditions: results from the WHO World Mental Health surveys. *Molecular Psychiatry*, **16**(12): 1234−1246.

Altinay M, Karne H, Anand A. 2018. Lithium monotherapy associated clinical improvement effects on amygdala-ventromedial prefrontal cortex resting state connectivity in bipolar disorder. *Journal of Affective Disorders*, **225**: 4−12.

Ates N, Caglayan A, Balcikanli Z, Sertel E, Beker MC, Dilsiz P, et al. 2022. Phosphorylation of PI3K/Akt at Thr308, but not phosphorylation of MAPK kinase, mediates lithium-induced neuroprotection against cerebral ischemia in mice. *Experimental Neurology*, **351**: 113996.

Beaulieu JM, Marion S, Rodriguiz RM, Medvedev IO, Sotnikova TD, Ghisi V, et al. 2008. A β-arrestin 2 signaling complex mediates lithium action on behavior. *Cell*, **132**(1): 125−136.

Beaulieu JM, Sotnikova TD, Yao WD, Kockeritz L, Woodgett JR, Gainetdinov RR, et al. 2004. Lithium antagonizes dopamine-dependent behaviors mediated by an AKT/glycogen synthase kinase 3 signaling cascade. *Proceedings of the National Academy of Sciences of the United States of America*, **101**(14): 5099−5104.

Bjertrup A, Macoveanu J, Laurent H, Moszkowicz M, Finnegan MK, Egmose I, et al. 2022. Reduced prefrontal cortex response to own vs. unknown emotional infant faces in mothers with bipolar disorder. *European*

Neuropsychopharmacology, **54**: 7−20.

Cardoso G, Xavier M, Vilagut G, Petukhova M, Alonso J, Kessler RC, et al. 2018. Days out of role due to common physical and mental conditions in Portugal: results from the WHO World Mental Health Survey. *BJPsych Open*, **3**(1): 15−21.

Cavalleri L, Merlo Pich E, Millan MJ, Chiamulera C, Kunath T, Spano PF, et al. 2018. Ketamine enhances structural plasticity in mouse mesencephalic and human iPSC-derived dopaminergic neurons via AMPAR-driven BDNF and mTOR signaling. *Molecular Psychiatry*, **23**(4): 812−823.

Chai XJ, Whitfield-Gabrieli S, Shinn AK, Gabrieli JDE, Nieto Castañón A, Mccarthy JM, et al. 2011. Abnormal medial prefrontal cortex resting-state connectivity in bipolar disorder and schizophrenia. *Neuropsychopharmacology*, **36**(10): 2009−2017.

Chaves Filho AJM, Cunha NL, De Souza AG, Soares MVR, Jucá PM, De Queiroz T, et al. 2020. The GLP-1 receptor agonist liraglutide reverses mania-like alterations and memory deficits induced by D-amphetamine and augments lithium effects in mice: relevance for bipolar disorder. *Progress in Neuro-Psychopharmacology and Biological Psychiatry*, **99**: 109872.

Coggeshall RE, Lekan HA. 1996. Methods for determining numbers of cells and synapses: a case for more uniform standards of review. *Journal of Comparative Neurology*, **364**(1): 6−15.

Crawford CA, Moran AE, Baum TJ, Apodaca MG, Montejano NR, Park GI, et al. 2020. Effects of monoamine depletion on the ketamine-induced locomotor activity of preweanling, adolescent, and adult rats: sex and age differences. *Behavioural Brain Research*, **379**: 112267.

Dawson GR, Tricklebank MD. 1995. Use of the elevated plus maze in the search for novel anxiolytic agents. *Trends in Pharmacological Sciences*, **16**(2): 33−36.

Debom G, Gazal M, Soares MSP, Do Couto CAT, Mattos B, Lencina C, et al. 2016. Preventive effects of blueberry extract on behavioral and biochemical dysfunctions in rats submitted to a model of manic behavior induced by ketamine. *Brain Research Bulletin*, **127**: 260−269.

Ding XY, Chang YJ, Wang SQ, Yan D, Yao JK, Zhu GQ. 2021. Transcriptomic analysis of the effect of GAT-2 deficiency on differentiation of mice naïve T cells into Th1 cells *in vitro*. *Frontiers in Immunology*, **12**: 667136.

Ettenberg A, Ayala K, Krug JT, Collins L, Mayes MS, Fisher MPA. 2020. Differential effects of lithium isotopes in a ketamine-induced hyperactivity model of mania. *Pharmacology Biochemistry and Behavior*, **190**: 172875.

Franklin KBJ, Paxinos G. 2007. The Mouse Brain in Stereotaxic Coordinates. 3rd ed. Pittsburgh: Academic Press.

Gao TH, Ni RJ, Liu SS, Tian Y, Wei JX, Zhao LS, et al. 2021. Chronic lithium exposure attenuates ketamine-induced mania-like behavior and c-Fos expression in the forebrain of mice. *Pharmacology Biochemistry and Behavior*, **202**: 173108.

Ghedim FV, De B. Fraga D, Deroza PF, Oliveira MB, Valvassori SS, Steckert AV, et al. 2012. Evaluation of behavioral and neurochemical changes induced by ketamine in rats: implications as an animal model of mania. *Journal of Psychiatric Research*, **46**(12): 1569−1575.

Grande I, Berk M, Birmaher B, Vieta E. 2016. Bipolar disorder. *The Lancet*, **387**(10027): 1561−1572.

Hadamitzky M, Herring A, Kirchhof J, Bendix I, Haight MJ, Keyvani K, et al. 2018. Repeated systemic treatment with rapamycin affects behavior and amygdala protein expression in rats. *International Journal of Neuropsychopharmacology*, **21**(6): 592−602.

Hajek T, Bauer M, Pfennig A, Cullis J, Ploch J, O'Donovan C, et al. 2012. Large positive effect of lithium on prefrontal cortex *N*-acetylaspartate in patients with bipolar disorder: 2-centre study. *Journal of Psychiatry and Neuroscience*, **37**(3): 185−192.

He XX, Li M, Yu HM, Liu GJ, Wang NN, Yin CZ, et al. 2020. Loss of hepatic aldolase B activates Akt and promotes hepatocellular carcinogenesis by destabilizing the Aldob/Akt/PP2A protein complex. *PLoS Biology*, **18**(12): e3000803.

Hermida MA, Dinesh Kumar J, Leslie NR. 2017. GSK3 and its interactions with the PI3K/AKT/mTOR signalling network. *Advances in Biological Regulation*, **65**: 5−15.

Hopkins HS, Gelenberg AJ. 2000. Serum lithium levels and the outcome of maintenance therapy of bipolar disorder. *Bipolar Disorders*, **2**(3 Pt 1): 174–179.

Hu YL, Kung S, Ozerdem A, Vande Voort JL, Singh B, McDonald WM, et al. 2021. Hypomania associated with high dose ketamine treatment. *Bipolar Disorders*, **23**(4): 426−428.

Ishii N, Terao T, Hirakawa H. 2021. The present state of lithium for the prevention of dementia related to alzheimer's dementia in clinical and epidemiological studies: a critical review. *International Journal of Environmental Research and Public Health*, **18**(15): 7756.

Katz IR, Rogers MP, Lew R, Thwin SS, Doros G, Ahearn E, et al. 2022. Lithium treatment in the prevention of repeat suicide-related outcomes in veterans with major depression or bipolar disorder: a randomized clinical trial. *JAMA Psychiatry*, **79**(1): 24−32.

Khakpai F, Ebrahimi-Ghiri M, Alijanpour S, Zarrindast MR. 2019. Ketamine-induced antidepressant like effects in mice: a possible involvement of cannabinoid system. *Biomedicine & Pharmacotherapy*, **112**: 108717.

Krug JT, Klein AK, Purvis EM, Ayala K, Mayes MS, Collins L, et al. 2019. Effects of chronic lithium exposure in a modified rodent ketamine-induced hyperactivity model of mania. *Pharmacology Biochemistry and Behavior*, **179**: 150−155.

Li HJ, Su X, Zhang LW, Zhang CY, Wang L, Li WQ, et al. 2020. Transcriptomic analyses of humans and mice provide insights into depression. *Zoological Research*, **41**(6): 632−643.

Li M, Wang X, Ma RR, Shi DB, Wang YW, Li XM, et al. 2019. The olfactory receptor family 2, subfamily T, member 6 (OR2T6) is involved in breast cancer progression via initiating epithelial-mesenchymal transition and MAPK/ERK pathway. *Frontiers in Oncology*, **9**: 1210.

Li NX, Lee B, Liu RJ, Banasr M, Dwyer JM, Iwata M, et al. 2010. mTOR-dependent synapse formation underlies the rapid antidepressant effects of NMDA antagonists. *Science*, **329**(5994): 959−964.

Liu RJ, Fuchikami M, Dwyer JM, Lepack AE, Duman RS, Aghajanian GK. 2013. GSK-3 inhibition potentiates the synaptogenic and antidepressant-like effects of subthreshold doses of ketamine. *Neuropsychopharmacology*, **38**(11): 2268−2277.

Machado-Vieira R, Zanetti MV, Teixeira AL, Uno M, Valiengo LL, Soeiro-De-Souza MG, et al. 2015. Decreased AKT1/mTOR pathway mRNA expression in short-term bipolar disorder. *European Neuropsychopharmacology*, **25**(4): 468−473.

Malhi GS, Outhred T. 2016. Therapeutic mechanisms of lithium in bipolar disorder: recent advances and current understanding. *CNS Drugs*, **30**(10): 931−949.

Mandyam MC, Ahuja NK. 2017. Ketamine-induced mania during treatment for complex regional pain syndrome. *Pain Medicine*, **18**(10): 2040−2041.

McInnes LA, James-Myers MB, Turner MS. 2016. Possible affective switch associated with intravenous ketamine treatment in a patient with bipolar I

disorder. *Biological Psychiatry*, **79**(9): e71−e72.
Morrison JM Jr, Pritchard HD, Braude MC, D'Aguanno W. 1971. Plasma and brain lithium levels after lithium carbonate and lithium chloride administration by different routes in rats. *Proceedings of the Society for Experimental Biology and Medicine*, **137**(3): 889−892.
Ni RJ, Huang ZH, Luo PH, Ma XH, Li T, Zhou JN. 2018. The tree shrew cerebellum atlas: systematic nomenclature, neurochemical characterization, and afferent projections. *Journal of Comparative Neurology*, **526**(17): 2744−2775.
Ni RJ, Tian Y, Dai XY, Zhao LS, Wei JX, Zhou JN, et al. 2020a. Social avoidance behavior in male tree shrews and prosocial behavior in male mice toward unfamiliar conspecifics in the laboratory. *Zoological Research*, **41**(3): 258−272.
Ni RJ, Wang J, Shu YM, Xu L, Zhou JN. 2020b. Mapping of c-Fos expression in male tree shrew forebrain. *Neuroscience Letters*, **714**: 134603.
Nichols SD, Bulman M, Tisher A, Campbell III JJ. 2016. A Case of possible iatrogenic ketamine-induced mania in a patient being treated for postoperative pain. *Psychosomatics*, **57**(5): 543−546.
Openshaw RL, Thomson DM, Thompson R, Penninger JM, Pratt JA, Morris BJ, et al. 2020. *Map2k7* haploinsufficiency induces brain imaging endophenotypes and behavioral phenotypes relevant to schizophrenia. *Schizophrenia Bulletin*, **46**(1): 211−223.
Pan JQ, Lewis MC, Ketterman JK, Clore EL, Riley M, Richards KR, et al. 2011. AKT kinase activity is required for lithium to modulate mood-related behaviors in mice. *Neuropsychopharmacology*, **36**(7): 1397−1411.
Parise EM, Parise LF, Sial OK, Cardona-Acosta AM, Gyles TM, Juarez B, et al. 2021. The resilient phenotype induced by prophylactic ketamine exposure during adolescence is mediated by the ventral tegmental area-nucleus accumbens pathway. *Biological Psychiatry*, **90**(7): 482−493.
Prickaerts J, Moechars D, Cryns K, Lenaerts I, Van Craenendonck H, Goris I, et al. 2006. Transgenic mice overexpressing glycogen synthase kinase 3β: a putative model of hyperactivity and mania. *Journal of Neuroscience*, **26**(35): 9022−9029.
Qin ZH, Zhang L, Zasloff MA, Stewart AFR, Chen HH. 2021. Ketamine's schizophrenia-like effects are prevented by targeting PTP1B. *Neurobiology of Disease*, **155**: 105397.
Radford KD, Park TY, Lee BH, Moran S, Osborne LA, Choi KH. 2017. Dose-response characteristics of intravenous ketamine on dissociative stereotypy, locomotion, sensorimotor gating, and nociception in male Sprague-Dawley rats. *Pharmacology Biochemistry and Behavior*, **153**: 130−140.
Ricke AK, Snook RJ, Anand A. 2011. Induction of prolonged mania during ketamine therapy for reflex sympathetic dystrophy. *Biological Psychiatry*, **70**(4): e13−e14.
Savitz JB, Price JL, Drevets WC. 2014. Neuropathological and neuromorphometric abnormalities in bipolar disorder: view from the medial prefrontal cortical network. *Neuroscience & Biobehavioral Reviews*, **42**: 132−147.
Shin EJ, Nguyen BT, Jeong JH, Hoai Nguyen BC, Tran NKC, Sharma N, et al. 2021. Ouabain inhibitor rostafuroxin attenuates dextromethorphan-induced manic potential. *Food and Chemical Toxicology*, **158**: 112657.
Shvartsur R, Agam G, Uzzan S, Azab AN. 2022. Low-dose aspirin augments the anti-inflammatory effects of low-dose lithium in lipopolysaccharide-treated rats. *Pharmaceutics*, **14**(5): 901.
Spohr L, Soares MSP, Bona NP, Pedra NS, Barschak AG, Alvariz RM, et al. 2022. Effect of blueberry extract on energetic metabolism, levels of brain-derived neurotrophic factor, and Ca^{2+}-ATPase activity in the hippocampus and cerebral cortex of rats submitted to ketamine-induced mania-like behavior. *Metabolic Brain Disease*, **37**(3): 835−847.
Su WR, Wan Q, Han LH, Huang JW, Chen XQ, Chen GH, et al. 2014. Doxycycline exerts multiple anti-allergy effects to attenuate murine allergic conjunctivitis and systemic anaphylaxis. *Biochemical Pharmacology*, **91**(3): 359−368.
Urs NM, Snyder JC, Jacobsen JPR, Peterson SM, Caron MG. 2012. Deletion of GSK3β in D2R-expressing neurons reveals distinct roles for β-arrestin signaling in antipsychotic and lithium action. *Proceedings of the National Academy of Sciences of the United States of America*, **109**(50): 20732−20737.
Valvassori SS, Dal-Pont GC, Resende WR, Jornada LK, Peterle BR, Machado AG, et al. 2017. Lithium and valproate act on the GSK-3β signaling pathway to reverse manic-like behavior in an animal model of mania induced by ouabain. *Neuropharmacology*, **117**: 447−459.
Vanderplow AM, Eagle AL, Kermath BA, Bjornson KJ, Robison AJ, Cahill ME. 2021. Akt-mTOR hypoactivity in bipolar disorder gives rise to cognitive impairments associated with altered neuronal structure and function. *Neuron*, **109**(9): 1479−1496.e6.
Wu CH, Wang Y, He Y, Wu S, Xie ZF, Zhang J, et al. 2020. Sub-anesthetic and anesthetic ketamine produce different long-lasting behavioral phenotypes (24 h post-treatment) via inducing different brain-derived neurotrophic factor (BDNF) expression level in the hippocampus. *Neurobiology of Learning and Memory*, **167**: 107136.
Xing XL, Zhang J, Wu KY, Cao BB, Li XF, Jiang F, et al. 2019. Suppression of Akt-mTOR pathway rescued the social behavior in *Cntnap2*-deficient mice. *Scientific Reports*, **9**(1): 3041.
Xiu J, Zhang Q, Zhou T, Zhou TT, Chen Y, Hu HL. 2014. Visualizing an emotional valence map in the limbic forebrain by TAI-FISH. *Nature Neuroscience*, **17**(11): 1552−1559.
Yang ZH, Cai X, Qu N, Zhao LJ, Zhong BL, Zhang SF, et al. 2020. Identification of a functional 339 bp Alu insertion polymorphism in the schizophrenia-associated locus at 10q24.32. *Zoological Research*, **41**(1): 84−89.
Ye MS, Zhang JY, Yu DD, Xu M, Xu L, Lv LB, et al. 2021. Comprehensive annotation of the Chinese tree shrew genome by large-scale RNA sequencing and long-read isoform sequencing. *Zoological Research*, **42**(6): 692−709.
Young JW, Henry BL, Geyer MA. 2011. Predictive animal models of mania: hits, misses and future directions. *British Journal of Pharmacology*, **164**(4): 1263−1284.
Zhang CL, Li YJ, Lu S, Zhang T, Xiao R, Luo HR. 2021. Fluoxetine ameliorates depressive symptoms by regulating lncRNA expression in the mouse hippocampus. *Zoological Research*, **42**(1): 28−42.
Zhou W, Wang N, Yang C, Li XM, Zhou ZQ, Yang JJ. 2014. Ketamine-induced antidepressant effects are associated with AMPA receptors-mediated upregulation of mTOR and BDNF in rat hippocampus and prefrontal cortex. *European Psychiatry*, **29**(7): 419−423.
Zhang WW, Jia P, Lu XB, Chen XQ, Weng JH, Jia KT, et al. 2022. Capsid protein from red-spotted grouper nervous necrosis virus induces incomplete autophagy by inactivating the HSP90ab1-AKT-MTOR pathway. *Zoological Research*, **43**(1): 98−110.